An Empirical Study of the Effects of Flux Reconstruction on the FVFD Solution of Maxwell's Equations on Unstructured Grids

Ian Jeffrey and Joe LoVetri

Department of Electrical and Computer Engineering
University of Manitoba, Winnipeg, MB, R3T 5V6, Canada
ijeffrey@ee.umanitoba.ca, Joe_LoVetri@umanitoba.ca

Abstract: In this paper, we empirically study the effects of flux-reconstruction schemes on the iterative solution to a spatially collocated, upwind, finite-volume frequency-domain (FVFD) formulation of Maxwell's equations. The FVFD algorithm is obtained from the continuous finite-volume time-domain (FVTD) equations through time-harmonic assumptions suggesting that the FVFD spatial error is inherited from FVTD and is dependent on the flux-reconstruction scheme selected. By investigating the convergence rate and solution error of first-order, harmonic, and MUSCL solutions to a PEC scattering problem we show that a hybrid solution that uses a first-order flux solution as an initial guess to the MUSCL solution may be one way to improve the iterative convergence.

Keywords: Finite-Volume Frequency Domain, Finite-Volume Time-Domain, Flux Reconstruction

1. Introduction

Over the past two decades, the finite-volume time-domain (FVTD) numerical method for solving Maxwell's Equations has been applied to a variety of field problems with much success [1-4]. While FVTD is capable of producing broad-band system response in a single execution, long run-times may be required to obtain a desired frequency resolution. When discrete frequency solutions are required (e.g. in the field of microwave tomography for biomedical imaging [5]), a frequency-domain solution may be more efficient. The finite-volume frequency-domain (FVFD) formulation of Maxwell's equations is obtained directly from FVTD under time-harmonic assumptions and since its apparent introduction in [6] has begun to garner attention due to its geometric modeling capabilities [7]. Two attractive features of the FVFD method are that the numerical algorithm is easily implemented from existing FVTD codes and that both the electric and magnetic field components are computed directly by the algorithm. On the other hand, an FVFD solution to Maxwell's equations requires solving a matrix equation. For real-world problems, a direct inversion of the resulting system matrix is prohibitive and iterative techniques must be employed. In this case, the computational time becomes dependent on the matrix conditioning.

In this paper, we study the effects of standard flux-reconstruction approximations on the accuracy and convergence rate of the iterative solution to the FVFD formulation. The FVFD numerical scheme is briefly formulated for Maxwell's equations and a variety of boundary-flux reconstruction

schemes are discussed. Numerical results displaying the accuracy and convergence rate of the FVFD algorithm are provided for scattering from a PEC sphere. The possibility of using a combination of reconstruction schemes to improve convergence is investigated.

2. The Finite-Volume Frequency-Domain Algorithm

To formulate the FVFD algorithm, it is assumed that a finite computational domain V is partitioned into N_V first-order polyhedral finite-volumes (or cells) V_i each having an associated volume $|V_i|$. The barycentre of the i^{th} volume is denoted by $\vec{r}_i$. Each polyhedral volume is bounded by a set of K_i flat facets symbolized by $\partial V_{i,k}$. It is assumed that the material parameters associated with the i^{th} volume are constants: the permittivity in the i^{th} cell is ϵ_i [F/m], the permeability is μ_i [H/m], and the conductivity is σ_i [S/m]. In the case of a scattered-field formulation, the background constitutive parameters are, also, assumed to be constant on a cell and are denoted by ϵ_{i_b}, μ_{i_b} and σ_{i_b}. The FVFD algorithm aims to numerically solve a surface-volume formulation of Maxwell's equations, obtained by integrating Maxwell's curl equations and applying the divergence theorem [6]:

$$(j\omega\bar{\bar{\boldsymbol{I}}} - \bar{\bar{\boldsymbol{\alpha}}}_i^{-1} \cdot \bar{\bar{\boldsymbol{\sigma}}}_i) \cdot \vec{\boldsymbol{U}}_i + \frac{1}{|V_i|} \sum_{k=1}^{K_i} \iint_{\partial V_{i,k}} \bar{\bar{\boldsymbol{A}}}_{i,k} \cdot \vec{\boldsymbol{U}}(\vec{r}) dS = \bar{\bar{\boldsymbol{\alpha}}}_i^{-1} \cdot \vec{\boldsymbol{S}}_i. \tag{1}$$

The solution vector $\vec{\boldsymbol{U}}(\vec{r}) \in \mathbb{R}^6$ at position $\vec{r}$ is given by $\vec{\boldsymbol{U}}(\vec{r}) = [\vec{E}(\vec{r})^t \ \vec{H}(\vec{r})^t]^t$ where the electric field $\vec{E}(\vec{r})$ [V/m] and magnetic field $\vec{H}(\vec{r})$ [A/m] are assumed time-harmonic at radial frequency ω [rad/s] under the assumption of an $\exp(j\omega t)$ time-dependence with $j = \sqrt{-1}$. Subscripted vector quantities such as $\vec{\boldsymbol{U}}_i$ denote a volume average over V_i. Under a scattered-field formulation $\vec{\boldsymbol{U}}(\vec{r})$ is understood to represent scattered fields. The constitutive parameters are accounted for by the two constant 6×6 matrices associated with the i^{th} cell:

$$\bar{\bar{\boldsymbol{\alpha}}}_i = \text{diag}\{\epsilon_i \ \epsilon_i \ \epsilon_i \ \mu_i \ \mu_i \ \mu_i\} \quad \bar{\bar{\boldsymbol{\sigma}}}_i = \text{diag}\{\text{-}\sigma_i \ \text{-}\sigma_i \ \text{-}\sigma_i \ 0 \ 0 \ 0\}. \tag{2}$$

The surface integral is interpreted as the flux of the solution $\vec{\boldsymbol{U}}(\vec{r})$ over ∂V_i where the flux matrix $\bar{\bar{\boldsymbol{A}}}_{i,k}$ on facet k of cell i is a function of the outward unit normal to the surface, ϵ_i and μ_i. Electromagnetic boundary conditions (including mesh truncation) are easily enforced by appropriate modifications of the flux matrix. These details will not be provided herein but may be found in [1]. Finally, under a total-field formulation, the source term $\vec{\boldsymbol{S}}(\vec{r}) = [-\vec{J}(\vec{r})^t \ \vec{0}^t]^t$ where $\vec{J}(\vec{r})$ [A/m^2] is the time-harmonic current density. Under a scattered-field formulation the source vector in the i^{th} cell is a function of the incident fields $\vec{\boldsymbol{U}}^{inc}(\vec{r})$ that are assumed to be supported by the current density $\vec{J}(\vec{r})$:

$$\vec{\boldsymbol{S}}(\vec{r}) = -(\bar{\bar{\boldsymbol{\alpha}}}_i - \bar{\bar{\boldsymbol{\alpha}}}_{i_b}) \cdot j\omega\vec{\boldsymbol{U}}^{inc}(\vec{r}) + (\bar{\bar{\boldsymbol{\sigma}}}_i - \bar{\bar{\boldsymbol{\sigma}}}_{i_b}) \cdot \vec{\boldsymbol{U}}^{inc}(\vec{r}) \quad \forall \vec{r} \in V_i.$$

FVFD seeks to numerically solve (1) for the volumetric average $\vec{\boldsymbol{U}}_i$ on each cell. We limit ourselves to the second-order approximation that $\vec{\boldsymbol{U}}_i$, $\vec{\boldsymbol{S}}_i$ are, respectively, given by the barycentric values $\vec{\boldsymbol{U}}(\vec{r}_i)$ and $\vec{\boldsymbol{S}}(\vec{r}_i)$ on V_i. Consequently, we associate with each finite-volume the six unknown field quantities at its barycentre. The field values on the boundary of each volume are to be reconstructed from the barycentric values. Enforcing (1) on each cell in the domain V results in a sparse linear system of equations:

$$(\underline{\boldsymbol{M}} + \underline{\boldsymbol{S}} \cdot \underline{\boldsymbol{R}}) \cdot \mathbf{U} = \mathbf{S}, \tag{3}$$

where the $6N \times 6N$ mass matrix $\underline{\underline{\boldsymbol{M}}}$ contains the the left-hand-side of (1) for each finite-volume, the stiffness matrix $\underline{\underline{\boldsymbol{S}}}$ accounts for the surface integral operations (approximated to second-order by evaluating the integral at the centre of each facet making up the boundary) and the reconstruction matrix $\underline{\underline{\boldsymbol{R}}}$ accounts for the determination of the surface values from barycentric values. The $6N$-vectors $\mathbf{U}$ and $\mathbf{S}$ contain the solution and source terms for each cell, respectively. By inverting the matrix $\underline{\underline{\boldsymbol{M}}} + \underline{\underline{\boldsymbol{S}}} \cdot \underline{\underline{\boldsymbol{R}}}$ (iteratively), we obtain the fields at the barycentre of each volume.

3. Flux Reconstruction

In this section, we are concerned with the reconstruction of the solution $\vec{\boldsymbol{U}}(\vec{r})$ on the boundary of each surface element V_i from the barycentric solutions $\mathbf{U}$, *i.e.* we wish to evaluate $\underline{\underline{\boldsymbol{R}}} \cdot \mathbf{U}$. The FVTD implementation used to develop our FVFD algorithm is a flux-split, upwind solver. This implies that the evaluation of the surface flux $\bar{\bar{\boldsymbol{A}}}_{i,k} \cdot \vec{\boldsymbol{U}}(\vec{r})$, $\vec{r} \in \partial V_{i,k}$ is decomposed into an outgoing and incoming flux as:

$$\bar{\bar{\boldsymbol{A}}}_{i,k} \cdot \vec{\boldsymbol{U}}(\vec{r}) = \bar{\bar{\boldsymbol{A}}}^{+}_{i,k} \cdot \vec{\boldsymbol{U}}^{+}(\vec{r}) + \bar{\bar{\boldsymbol{A}}}^{-}_{i,k} \cdot \vec{\boldsymbol{U}}^{-}(\vec{r}), \quad \vec{r} \in \partial V_{i,k}, \tag{4}$$

where $\vec{\boldsymbol{U}}^{+}(\vec{r})$ is the value of the solution on the facet interpolated from inside volume i while $\vec{\boldsymbol{U}}^{-}(\vec{r})$ is the value of the solution on the facet interpolated from the cell V_m that neighbours V_i on facet k (details are available in [4]). We note that flux reconstruction schemes generally alter the underlying system of partial differential equations by introducing diffusive, dispersive, or dissipative error terms depending on the type of reconstruction [8]. We now consider different ways of approximating the fields on $\partial V_{i,k}$.

3.1. First-Order Reconstruction

The simplest reconstruction possible is the first-order reconstruction that simply the cell-centered solutions to the boundary values. If V_m neighbours V_i at $\vec{r}$ we have:

$$\begin{aligned} \vec{\boldsymbol{U}}^{+}(\vec{r}) &= \vec{\boldsymbol{U}}_i \\ \vec{\boldsymbol{U}}^{-}(\vec{r}) &= \vec{\boldsymbol{U}}_m. \end{aligned} \tag{5}$$

In the time-domain, this first-order approximation leads to unacceptable numerical dissipation and is rarely used in practice. In the frequency domain, this results in a minimized coupling between sources and distant locations. While this will reduce the overall accuracy of the solution, it should be noted that in the proximity of sources it may yield reasonable approximate solutions.

3.2. Time-Harmonic Characteristic Reconstruction

As an alternative to the simple first-order reconstruction described above, an alternative method is to use the method of characteristics to account for the phase change between the cell-centered values $\vec{\boldsymbol{U}}_i$ located at $\vec{r}_i$ and the boundary evaluation point $\vec{r}$ [6]:

$$\begin{aligned} \vec{\boldsymbol{U}}^{+}(\vec{r}) &= \vec{\boldsymbol{U}}_i \exp(-j\omega\sqrt{\epsilon_i \mu_i}|\vec{r} - \vec{r}_i|) \\ \vec{\boldsymbol{U}}^{-}(\vec{r}) &= \vec{\boldsymbol{U}}_m \exp(-j\omega\sqrt{\epsilon_m \mu_m}|\vec{r} - \vec{r}_m|). \end{aligned} \tag{6}$$

This reconstruction is slightly more computationally expensive than the first-order implementation and is not strictly second order accurate. We might interpret it as lying somewhere between first- and second-order accuracy.

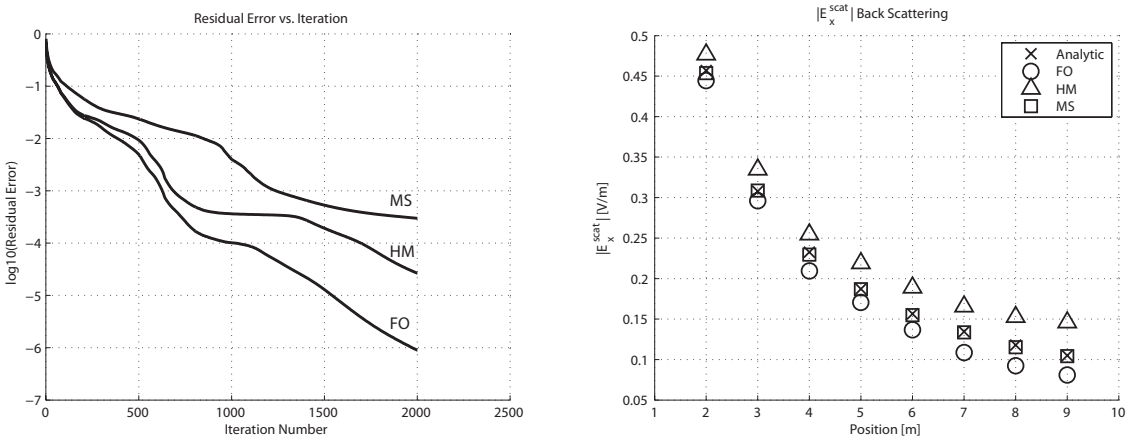

(a) (b)

Fig. 1. (a) FVFD GMRES convergence rate for different flux reconstruction schemes. (b) Backscattered solution for different flux reconstruction schemes. The analytic solution is provided for reference.

3.3. MUSCL Reconstruction

To obtain a second-order accurate spatial reconstruction, we use the *monotone upwind scheme for conservation laws* (MUSCL). In this scheme, the cell boundary values are reconstructed to second-order by first computing the gradient of the solution for each cell-center and then using Taylor's theorem [1]:

$$\begin{aligned}(\vec{\boldsymbol{U}}(\vec{r})^{+})_p &= (\vec{\boldsymbol{U}}_i)_p + (\vec{r} - \vec{r}_i) \cdot \nabla(\vec{\boldsymbol{U}}_i)_p \\ (\vec{\boldsymbol{U}}(\vec{r})^{-})_p &= (\vec{\boldsymbol{U}}_m)_p + (\vec{r} - \vec{r}_m) \cdot \nabla(\vec{\boldsymbol{U}}_m)_p,\end{aligned} \tag{7}$$

where the subscript p ranges over the six components of the solution vector in $V_{i/m}$. The gradient term is computed as a contour integral over the faces of V_i where the face values are approximated using a weighted-distance average of $(\vec{\boldsymbol{U}}_i)_p$ and the neighbouring element solutions. We note that the computation of the MUSCL gradient is more expensive than both of the previous schemes. Furthermore, the gradient increases the bandwidth of the reconstruction operator $\underline{\boldsymbol{R}}$ as the gradient operation requires information from the neighbours of neighbouring cells.

3.4. Central Reconstruction

As a final option, we mention a central approximation to the flux reconstruction:

$$\vec{\boldsymbol{U}}(\vec{r})^{+} = \vec{\boldsymbol{U}}(\vec{r})^{-} = \frac{\vec{\boldsymbol{U}}_i + \vec{\boldsymbol{U}}_j}{2}. \tag{8}$$

In the time-domain, this type of flux interpolation cannot be used in conjunction with a time-collocated upstream scheme, but may be used in a leap-frog scheme (e.g. [9]). A leap-frog-equivalent formulation in the frequency domain is not obvious so we do not consider this scheme further.

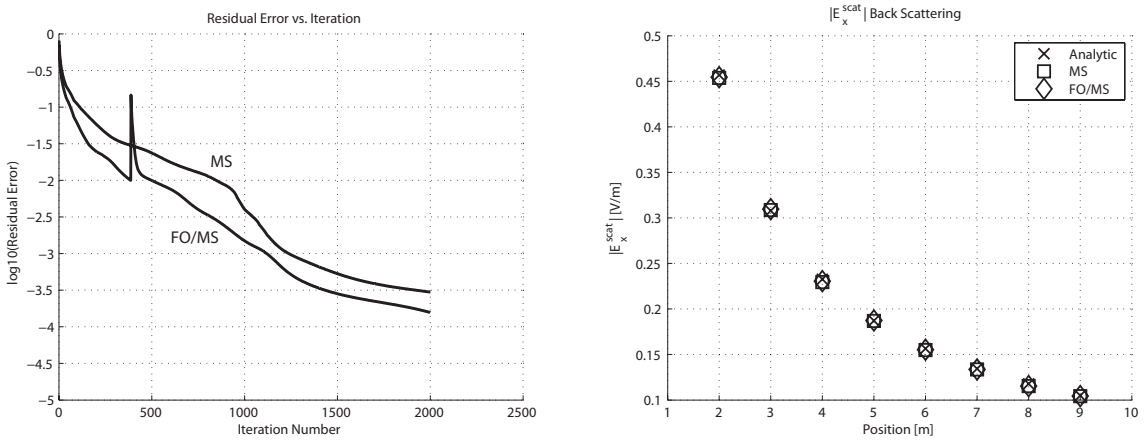

(a) (b)

Fig. 2. (a) FVFD GMRES convergence rate for the FO/MS hybrid scheme vs. the MS scheme. The discontinuity shows where the FO solution is used as an initial guess for the MS system. (b) Backscattered results for the FO/MS and MS systems.

4. Numerical Results

The conditioning of $\underline{\boldsymbol{M}} + \underline{\boldsymbol{S}} \cdot \underline{\boldsymbol{R}}$ is dependent on the reconstruction matrix $\underline{\boldsymbol{R}}$, and therefore the selected reconstruction scheme. To investigate the effects of the flux reconstruction on both the accuracy and iterative convergence of the FVFD algorithm, we simulate the problem of plane-wave scattering by a perfect-electric-conducting (PEC) sphere as it permits an analytic solution. We consider a 1 [m] radius PEC sphere centered in a 10 [m] radius spherical computational domain truncated with Silver-Müller absorbing boundaries [1]. The sphere was discretized with 2612 triangular facets while the discretized volume contains approximately 1.16 million first-order tetrahedral elements resulting in a problem size of roughly 7 million unknowns. As the mesh supports a maximum frequency of approximately 75 [MHz] at one-tenth of a wavelength, we compute the scattered field of a 50 [MHz] z-incident and x-polarized plane-wave. The iterative solution was obtained using GMRES without any preconditioning. This solver was selected over the BICGSTAB algorithm suggested in [6] simply because GMRES converges monotonically whereas BICGSTAB does not. Our FVFD implementation does not store the matrix but computes it on-the-fly and has been parallelized for distributed memory environments [10].

In Figure 1(a), we show the residual relative norm of the matrix equation as a function of GMRES iteration for the first-order (FO), harmonic (HM), and MUSCL (MS) reconstructions to 2000 iterations. In Figure 1(b), we show the reconstructed scattered field $|\bar{\mathcal{E}}_x^{scat}|$ at back-scatter locations from $z = 2$ [m] to $z = 9$ [m] in unit steps. The analytic solution is provided for reference. From the plots, we see that both the FO and HM solutions converge much faster than the MS reconstruction but to an inaccurate solution. The inaccuracies appear to increase away from the scatterer (sources). We note that the MS reconstruction is visually more accurate despite having a significantly higher residual after 2000 iterations.

Motivated by the quick convergence of the computationally less expensive FO reconstruction, we consider solving the matrix equation by first using the FO reconstruction to obtain an initial guess for the MS reconstruction. We denote this scheme as FO/MS. Figure 2(a) shows the convergence rate of a FO/MS scheme. The discontinuity of the convergence indicates the location where the

FO solution was used as an initial guess to the MS system. It is apparent that in the same number of iterations, the FO/MS scheme converges to a lower residual error than the MS scheme alone.

5. Conclusions and Future Work

Herein, we have empirically investigated the effects of first-order, harmonic, and MUSCL flux reconstruction schemes on the iterative convergence of the FVFD solution to Maxwell's equations. While low-order reconstructions converge faster than the MUSCL scheme, they do not accurately model the underlying system of differential equations. It has been demonstrated that (for the scattering problem considered herein) using a hybrid low-order/MUSCL solution can improve on the iterative convergence rate. Determining either an analytical or empirical rule for such hybrid schemes will be the focus of future work.

6. References

[1] P. Bonnet, X. Ferrières, B. Michielsen, and P. Lotz, "Finite-volume time-domain method," in *Time Domain Electromagnetics*, S. M. Rao, Ed. New York: Academic, 1997, pp. 307-367.

[2] C. Fumeaux, D. Baumann, and R. Vahldieck "Finite-Volume Time-Domain analysis of a cavity backed archimedean spiral antenna," *IEEE Transactions on Antennas and Propagation*, vol. 54, pp. 844-851, 2006.

[3] M. Yang, Y. Chen and R. Mittra, "Hybrid finite-difference/finite-volume time domain analysis for microwave integrated circuits with curved pec surfaces using a nonuniform rectangular grid," *IEEE Transactions on Microwave Theory and Techniques*, vol. 48, pp. 969-975, June 2000.

[4] D. Firsov, J. LoVetri, I. Jeffrey, V. Okhmatovski, C. Gilmore and W. Chamma, "High-order FVTD on unstructured grids using an object-oriented finite-volume time-domain computational engine," *ACES Journal*, vol. 22, no .1, pp. 71-82, March 2007.

[5] C. Gilmore, P. Mojabi and J. LoVetri, "Comparison of an Enhanced Distorted Born Iterative Method and the Multiplicative-Regularized Contrast Source Inversion Method," *IEEE Transactions on Antennas and Propagation*, vol. 57, no. 8, pp. 2341-2351, August 2009.

[6] P. Bonnet, X. Ferriéres, J. Grando, J.C. Alliot and J. Fontaine, "Frequency-Domain Finite Volume Method for Electromagnetic Scattering," *Antennas and Propagation Society Internation Symposium*, vol. 1, pp. 252-255, 1998.

[7] K. Krohne, D. Baumann, C. Fumeaux, E. Li, R. Vahldieck, "Frequency-Domain Finite-Volume Simulations," Proceedings of the 37th European Microwave Conference, pp. 158-161.

[8] R. J. LeVeque, *Finite Volume Methods for Hyperbolic Problems*, Cambridge, U.K.: Cambridge University Press, 2002.

[9] S. Piperno, M. Remaki, and L. Fezoui, "A nondiffusive finite volume scheme for the three-dimensional maxwell's equations on unstructured meshes," *SIAM Journal: Numerical Analysis*, vol. 39, no. 6, pp. 2089-2108.

[10] I. Jeffrey, D. Firsov, C. Gilmore, V. Okhmatovski, and J. LoVetri, "Parallel higher-order EM-FVTD on an unstructured mesh," *ACES* Conference, Verona, Italy, March 2007.